

Ballistic orbits in Schwarzschild space-time and gravitational waves from EMR binary mergers

G. d'Ambrosi^a and J.W. van Holten^b

NIKHEF
Amsterdam NL

July 2, 2014

Abstract

We describe a special class of ballistic geodesics in Schwarzschild space-time, extending to the horizon in the infinite past and future of observer time, which are characterized by the property that they are in 1-1 correspondence, and completely degenerate in energy and angular momentum, with stable circular orbits. We derive analytic expressions for the source terms in the Regge-Wheeler and Zerilli-Moncrief equations for a point-particle moving on such a ballistic orbit, and compute the gravitational waves emitted during the infall in an Extreme Mass Ratio black-hole binary coalescence. In this way a geodesic approximation to the plunge phase of compact binaries is obtained.

^a e-mail: gdambros@nikhef.nl

^b e-mail: v.holten@nikhef.nl

1 Introduction

The physics of black holes has become a subject of intense interest, pursued in theoretical and observational research by physicists and astronomers. One of the most promising roads to explore large black holes is by the detection of gravitational radiation from their interaction with compact objects, including other black holes.

It is widely expected that in the next decade the detection of gravitational waves of astrophysical origin will become a reality. Experimental evidence is to come from the ground-based interferometers LIGO and VIRGO [1, 2] as well as from the future missions eLISA and DECIGO [3]. Binary systems including a black hole are among the most prominent potential sources for detection.

The class of Extreme Mass-Ratio binaries (EMRs), in which a black hole of large mass M is accompanied by a compact object of much smaller mass μ , such that $\mu/M \ll 1$, is of particular interest because the compact object acts in many respects as a point-like probe of the black-hole geometry. From the theoretical point of view, compact binaries like these can be studied via perturbative methods, with the static or stationary black-hole solutions of General Relativity as a first-order approximation [4, 5].

Analytical results for the orbits of test masses in Schwarzschild space-time are found in standard text books [6, 7, 8]. Complete geodesics –meaning the full space-time position as a function of (proper) time– are less easy to compute, and usually given only in the form of implicit expressions. For practical applications several perturbative schemes have been developed to construct satisfactory approximations. The post-newtonian expansion, computing relativistic corrections to Kepler orbits, has been developed to high order in the parameters¹ v/c and GM/rc^2 ; see refs. [9, 10] and work cited there. In refs. [12, 13, 14, 15] a different, fully relativistic scheme has been developed based on covariant deformation of known (circular) orbits. This last method, developed to second order in the deformation parameter, was also shown to give very good results for the gravitational wave signals from quasi-periodic bound orbits with moderate eccentricities.

In the present paper we extend the relativistic calculations to include a particular class of unstable orbits, describing test masses falling towards the horizon in the regime where the motion is no longer quasi-periodic. A well-known extreme case of infall is the straight plunge along a radial orbit, which was dealt with extensively in refs. [16, 17]. Here we focus on the opposite extreme, infall from a periodic orbit, in particular circular orbits close to the innermost stable circular orbit (ISCO).

Such unstable orbits are interesting on their own and shed light on the dynamics of EMRs, so they can also be used for the evaluation of gravitational radiation. It is known [19] that binary coalescences go through three different stages, which are commonly referred to as the inspiral, plunge and merger-ringdown. During the *inspiral* of an EMR binary, the smaller companion μ follows bound quasi-periodic orbits, such as those studied in [13, 14, 15]. Loss of energy through GWs generally translates in a loss of eccentricity (*circularisation*) in this phase, although the eccentricity may increase again just before

¹In the remainder of this paper we use natural units $c = G = 1$.

plunging [18], depending on the parameters of the orbit and its evolution². However, the region of the ISCO is where the *plunge* sets in and the unstable orbits in some range of parameters can be used in the description of this phase and the following. In particular they show that an EMR plunge can follow an almost-circular path at the beginning, up to radial values $r \sim 4.3M$, when $\dot{r} \sim r\dot{\varphi}$ and the radial velocity becomes comparable to the transverse velocity, after which the radial motion becomes dominant. Moreover our particular unstable orbits may be the starting point for a geodesic deviation expansion [13, 14] which can give an even more realistic description of the final plunge of an EMR system.

This paper is organized as follows. In sect. 2 we review some elements of geodesic motion in Schwarzschild space-time, and show the existence of unstable infalling geodesics which are completely degenerate in energy and angular momentum per unit of mass with circular orbits. In particular, just like for the circular orbits (but approaching from the other side) the limit of stability of these geodesics is the ISCO. In sect. 3 we give explicit analytic relations between the space-time co-ordinates (t, r, φ) of an infalling test mass, including an expression for the proper time τ . In sect. 4 we use these results as input to derive expressions for the source terms in the Regge-Wheeler and Zerilli-Moncrief equations [20, 21, 22] for gravitational waves of a point mass in a Schwarzschild background. The wave equations are solved numerically using the Lousto-Price algorithm [23]. In the final section we discuss the results and compare them with similar results in the literature for infall from the ISCO.

2 Motion in Schwarzschild space-time

Time-like geodesics in the equatorial plane of Schwarzschild space-time are characterized by two constants of motion, the proper energy and angular momentum per unit of mass of a test particle:

$$\varepsilon = \left(1 - \frac{2M}{r}\right) \frac{dt}{d\tau}, \quad \ell = r^2 \frac{d\varphi}{d\tau}. \quad (1)$$

In terms of these the four-velocity constraint $u_\mu u^\mu = -1$ is equivalent to

$$\varepsilon^2 = \left(\frac{dr}{d\tau}\right)^2 + V_\ell(r), \quad (2)$$

with the effective potential

$$V_\ell = \left(1 - \frac{2M}{r}\right) \left(1 + \frac{\ell^2}{r^2}\right). \quad (3)$$

It follows, that for $\ell^2 > 12M^2$ there exist *circular* orbits with constant radial co-ordinate r . In fact, there are two types of circular orbits, a stable one at $r = R_+$ in the minimum

²However, the relative increase of the eccentricity is modest: $e \ll 1$, while during previous stages of the inspiral e can drop by orders of magnitude.

of V_ℓ , and an unstable one at $r = R_-$ in its maximum, with

$$R_\pm = \frac{\ell^2}{2M} \left(1 \pm \sqrt{1 - \frac{12M^2}{\ell^2}} \right). \quad (4)$$

For $R = 6M$ and $\ell^2 = 12M^2$ the effective potential V_ℓ only has a point of inflection, and these two solutions coincide; this is the well-known innermost stable circular orbit (ISCO). For $\ell^2 < 12M^2$ the potential V_ℓ has no stable points for any ℓ , and no circular orbits exist. The expression for V_ℓ for different circular orbits is conveniently parametrized by

$$\xi = \sqrt{1 - \frac{12M^2}{\ell^2}} \quad \Rightarrow \quad \varepsilon_\pm^2 = V_\ell[R_\pm] = \frac{2(2 \pm \xi)^2}{9(1 \pm \xi)}. \quad (5)$$

Note that for orbits near the ISCO (small ξ), both the energy and angular momentum of circular orbits vary only as ξ^2 . As a result, for orbits near the ISCO the effective potential is very flat between R_- and R_+ ; in fact, in the domain $\xi < 0.3$ the difference between maximum and minimum of V_ℓ is less than 1 percent.

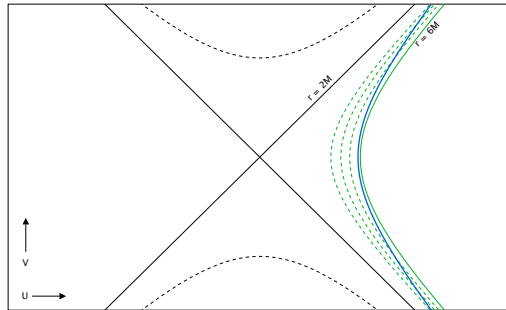


Fig. 1: Kruskal diagram showing a ballistic orbit crossing lines of constant $r < 6M$ (dotted curves). The ISCO ($r = 6M$) is the ultimate limit of ballistic orbits.

In this paper we consider a second class of unstable orbits. These orbits lie completely within the ISCO, starting from and falling back into the horizon; therefore we refer to them as *ballistic* orbits. An example is shown in fig. 1. We are especially interested in the class of orbits in 1-1-correspondence with circular geodesics, with the simple analytic representation

$$r = \frac{R}{1 + e \cotan^2(A\varphi/2)}. \quad (6)$$

Here (R, e, A) are constants fixed by the values of ε and ℓ . More precisely, just like for circular orbits, there is only one independent parameter fixing a ballistic orbit, which we can choose to be the extremal point (apastron) $r = R$ when $A\varphi = \pi$. Then the other

constants defining the ballistic orbit are

$$A^2 = \frac{1}{2} \left(\frac{6M}{R} - 1 \right), \quad e = \frac{3}{2} \left(1 - \frac{R}{6M} \right), \quad (7)$$

$$\varepsilon^2 = \frac{\left(1 + \frac{2M}{R}\right)^2}{1 + \frac{6M}{R}}, \quad \ell^2 = \frac{16M^2}{\left(1 - \frac{2M}{R}\right) \left(1 + \frac{6M}{R}\right)}.$$

It follows that these orbits only exist for $2M < R \leq 6M$, and the limiting case $R = 6M$ is just the ISCO itself, with $e = A = 0$. For these orbits the value of the parameter ξ , defined in (5), is

$$\xi = A^2 = \frac{1}{2} \left(\frac{6M}{R} - 1 \right), \quad (8)$$

from which it follows that

$$\varepsilon^2 = \frac{2(2 + \xi)^2}{9(1 + \xi)}. \quad (9)$$

Thus it is established that these ballistic orbits inside the ISCO are degenerate in energy and angular momentum with the stable circular orbits outside the ISCO; see fig. 2.

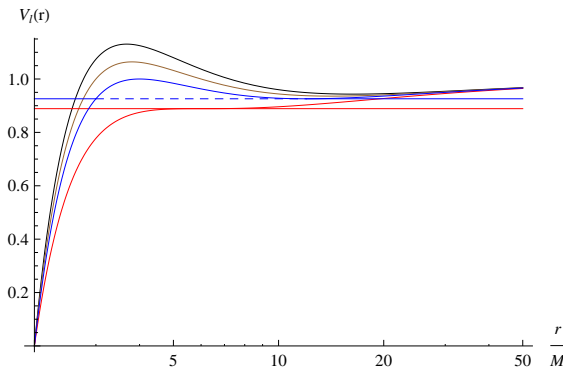


Fig. 2: $V_\ell(r)$ for several $\ell^2 \geq 12M^2$, where the equality sign determines the ISCO (lowest curve). The horizontal lines indicate the energy levels of the stable circular orbits (dashed) and corresponding ballistic orbits (continuous).

In summary, we have analytic representations for three kinds of special geodesics: stable and unstable circular orbits with respectively

$$R_+ = \frac{6M}{1 - \xi}, \quad R_- = \frac{6M}{1 + \xi}, \quad (10)$$

and special ballistic orbits with apastron

$$R = \frac{6M}{1 + 2\xi}. \quad (11)$$

These ballistic orbits are always degenerate in energy and angular momentum with the stable circular orbit for the same ξ , whilst the unstable circular orbit at this ξ has a slightly higher energy; however, all three become degenerate at the ISCO where $\xi = 0$. Other ballistic orbits exist; an analytic representation for these can be obtained from the ones given in eqs. (6) and (7) by the method of geodesic deviations [11, 12].

3 Infall on a ballistic orbit

As equation (6) is invariant under $\varphi \rightarrow -\varphi$, the ballistic orbit is symmetric about the apastron $r = R$. The second half of the orbit describes the infall of a test mass from the apastron to the horizon. Now the degeneracy in energy and angular momentum of the ballistic orbits and circular orbits implies that in both cases these quantities are greater than those of the ISCO. Thus it follows, that when a test particle in stable motion on the ISCO is slightly boosted with the correct angular momentum, it can either move up to a larger distance from the horizon on a stable circular orbit, or move down to such an infalling ballistic orbit of the same ε and ℓ . In real systems such a small boost could happen for instance by interaction with a third body passing by.

In this section we describe the infalling orbit in some more detail. First note, that eq. (6) expresses the radial co-ordinate r as a function of φ . By using the constants of motion (1) we can also determine the explicit functional dependence of the co-ordinate time t and the proper time τ on the angle φ . The expression for proper time is the simplest one; it is obtained by integrating the relation

$$\frac{d\varphi}{d\tau} = \frac{\ell}{r^2} = \frac{\ell}{R^2} \left(1 + e \cotan^2 \frac{A\varphi}{2} \right)^2, \quad (12)$$

with the result

$$\begin{aligned} \left(\frac{1-e}{(3-e)(3-2e)} \right)^{3/2} \frac{\tau - \tau_0}{2M} &= \frac{A\varphi}{(3-e)\sqrt{e}} - \arctan \left(\frac{1}{\sqrt{e}} \tan \frac{A\varphi}{2} \right) \\ &+ \frac{\sqrt{e}(1-e)}{3-e} \frac{\cotan \frac{A\varphi}{2}}{1 + e \cotan^2 \frac{A\varphi}{2}}. \end{aligned} \quad (13)$$

Here τ_0 is a constant of integration fixing the zero point of proper time. A convenient choice is to take $\tau = 0$ at $r = R$. Similarly, we can solve for t as a function of φ by integrating

$$\begin{aligned} \frac{dt}{d\varphi} &= \frac{\varepsilon}{\ell} \frac{r^3}{r - 2M} \\ &= \frac{2MR\varepsilon}{\ell} \left(\frac{R}{2M} \frac{1}{(1 + e \cotan^2 \frac{A\varphi}{2})^2} + \frac{1}{1 + e \cotan^2 \frac{A\varphi}{2}} + \frac{1}{\frac{R}{2M} - 1 - e \cotan^2 \frac{A\varphi}{2}} \right). \end{aligned} \quad (14)$$

The result is

$$\begin{aligned}
\frac{1}{(2-e)} \sqrt{\frac{e}{2(1-e)}} \frac{t-t_0}{4M} &= \frac{(3-2e)^2 A\varphi}{2(2-e)(1-e)^2} + \frac{e(3-2e)}{2(1-e)} \frac{\cotan \frac{A\varphi}{2}}{1+e \cotan^2 \frac{A\varphi}{2}} \\
&\quad - \frac{(11-11e+2e^2)\sqrt{e}}{2(1-e)^2} \arctan \left(\frac{1}{\sqrt{e}} \tan \frac{A\varphi}{2} \right) \\
&\quad - \frac{1}{(2-e)} \sqrt{\frac{e}{2(1-e)}} \operatorname{arccotanh} \left(\sqrt{\frac{2(1-e)}{e}} \tan \frac{A\varphi}{2} \right).
\end{aligned} \tag{15}$$

Finally, this result can be translated to a result for t as a function of r :

$$\begin{aligned}
\frac{2}{(2-e)} \sqrt{\frac{e}{2(1-e)}} \frac{t-t_0}{4M} &= \frac{(11-11e+2e^2)\sqrt{e}}{(1-e)^2} \arctan \sqrt{\frac{r}{(6-4e)M-r}} \\
&\quad - \frac{2(3-2e)^2}{(1-e)^2(2-e)} \arctan \sqrt{\frac{er}{(6-4e)M-r}} - \frac{\sqrt{er((6-4e)M-r)}}{2M(1-e)} \\
&\quad + \frac{1}{2-e} \sqrt{\frac{2e}{1-e}} \operatorname{arccotanh} \sqrt{\frac{2(1-e)r}{(6-4e)M-r}}.
\end{aligned} \tag{16}$$

A typical orbit close to the ISCO, with $e = 1.5 \times 10^{-3}$ is shown in fig. 3. This orbit encircles the black hole about 20 times before crossing the horizon. Moreover, the radial motion is seen to be small compared to the transverse motion until the radial co-ordinate gets in the domain $4M < r < 5M$. Once the cross-over to radially dominated motion is made, only a few turns remain. These observations will be made more precise in the following.

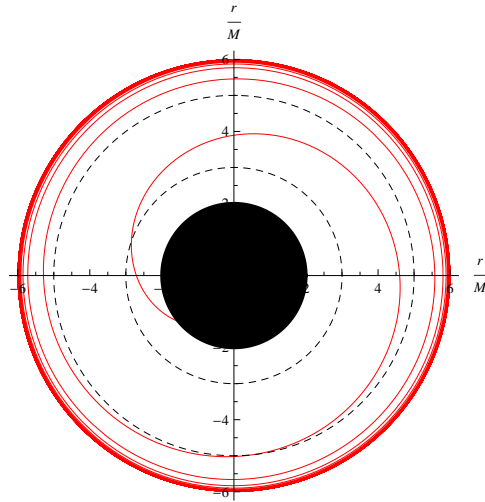


Fig. 3: The inspiralling ballistic orbit towards the Schwarzschild horizon for $e = 0.0015$.

4 Gravitational waves

When a test mass μ falls towards the horizon on a ballistic orbit, it emits gravitational waves. In this section we compute the gravitational wave signal and establish that the total energy radiated is only a small fraction of the energy of motion of the test body; therefore the motion on such a geodesic should be a reliable approximation to the exact orbit of an infalling compact object. It is then of interest to compare these calculations in the limit of small e with known results for the infall of a compact body from the ISCO.

Our computation of the gravitational wave signal for EMR systems is based on the Zerilli-Moncrief and Regge-Wheeler equations [20, 21, 22] for the angular modes of the linearized gravitational-wave forms $(\psi_{ZM}^{lm}, \psi_{RW}^{lm})$:

$$(\partial_{r^*}^2 - \partial_t^2 - \bar{V}_{ZM/RW}^l(r^*))\psi_{ZM/RW}^{lm} = \bar{S}_{ZM/RW}^{lm}, \quad (17)$$

where r^* represents the standard radial ‘tortoise’ co-ordinate

$$r^* = r + 2M \ln \left(\frac{r}{2M} - 1 \right),$$

whilst in terms of the original r -co-ordinate

$$\begin{aligned} \bar{V}_{ZM}^l &= \left(1 - \frac{2M}{r} \right) \frac{1}{r^2 \Lambda^2(r)} \left(2\lambda^2 \left(\lambda + 1 + \frac{3M}{r} \right) + \frac{18M^2}{r^2} \left(\lambda + \frac{M}{r} \right) \right), \\ \bar{V}_{RW}^l &= \left(1 - \frac{2M}{r} \right) \frac{1}{r^2} \left(l(l+1) - \frac{6M}{r} \right), \\ \lambda &= \frac{(l+2)(l-1)}{2} \quad \Lambda(r) = \lambda + \frac{3M}{r}. \end{aligned}$$

The expression for \bar{S}^{lm} on the right-hand side of eq. (17) represents the angular modes of the sources for the gravitational waves generated by the motion of the compact object in the black-hole background. Their explicit form is discussed in the appendix. The gravitational-wave amplitudes observed at large distance from the source can be reconstructed from the solutions for $\psi_{ZM/RW}^{lm}$ through the complex combination

$$h_+(r, t, \theta, \phi) - ih_\times(r, t, \theta, \phi) = \frac{1}{r} \sum_{l,m} \left(\psi_{ZM}^{lm}(r_{obs}^*, t) - 2i \int_{-\infty}^t \psi_{RW}^{lm}(r_{obs}^*, t') dt' \right) {}_{-2}Y^{lm}(\theta, \phi), \quad (18)$$

with (h_+, h_\times) the two independent circular polarization modes of the waves in the TT -gauge, and ${}_{-2}Y^{lm}(\theta, \phi)$ the spin-weighted spherical harmonics. The rates at which energy

and angular momentum are carried away by the gravitational waves are

$$\begin{aligned}
\frac{dE}{dt} &= \frac{1}{64\pi} \sum_{l,m} \frac{(l+2)!}{(l-2)!} \left(|\dot{\psi}_{ZM}^{lm}(r_{obs}^*, t)|^2 + 4|\dot{\psi}_{RW}^{lm}(r_{obs}^*, t)|^2 \right), \\
\frac{dL}{dt} &= 2 \operatorname{Re} \left[\frac{i}{128\pi} \sum_{l,m} m \frac{(l+2)!}{(l-2)!} \left(\dot{\psi}_{ZM}^{lm}(r_{obs}^*, t) \psi_{ZM}^{*lm}(r_{obs}^*, t) \right. \right. \\
&\quad \left. \left. + 4\dot{\psi}_{RW}^{*lm}(r_{obs}^*, t) \int_{-\infty}^t \psi_{RW}^{*lm}(r_{obs}^*, t') dt' \right) \right].
\end{aligned} \tag{19}$$

We have computed numerical solutions for the angular modes $\psi_{ZM/RW}^{lm}$ and the resulting metric perturbations $h_{+, \times}$, using a C++-implemented version of the Lousto-Price algorithm [16, 23]. The algorithm is based on dividing the (t, r^*) surfaces in Schwarzschild space-time into cells of equal area, which also represent cells of equal physical area. The differential equations (17) are discretized on this grid, and solutions are computed from appropriate initial conditions, such that further refinement of the grid does not change the result up to the desired accuracy.

To obtain a reliable wave signal for the infall on a ballistic orbit starting close to the ISCO from a quasi-periodic orbit, we consider a Schwarzschild space-time in which the inspiral of the test mass has produced a continuous set of outgoing gravitational waves. Realistic initial conditions for the angular modes $\psi_{ZM/RW}^{lm}$ are created by letting the test mass run on the ISCO for a sufficiently long period that any initial transient waves have passed the point where the observer is located and the wave forms are measured. We take this point to be in the equatorial plane at $r = 500M$.

Next we set the compact mass on a nearby ballistic orbit, and compute the resulting angular wave modes and metric perturbations. The instantaneous shift in the orbit, even if small, also produces a transient signal. However, for small e the ballistic orbit has an almost-periodic initial stage during which it runs close to the ISCO for a long time. During this time the original periodic signal is recovered to a very good approximation.

In fact, initial transients are common in standard numerical techniques, arising for example from the well-known Gibbs phenomenon [24, 25]. We have checked that changing the initial conditions in various ways, though affecting the transient signal, does not change the almost-periodic signal during the initial stage of the ballistic orbit, nor the development of the signal afterwards. Thus it is confirmed that, as in other numerical works [26, 27], spurious transients appear only in the initial phase of the signal and are followed by numerically stable physical wave forms.

Fig. 4 shows the results for the most relevant ZM- and RW-modes, as calculated for a system with mass ratio $\nu = \mu/M = 10^{-7}$ on a ballistic orbit with $e = 1.5 \times 10^3$, as observed from the equatorial plane. For convenience of representation the amplitudes have been rescaled by the inverse of the mass ratio.

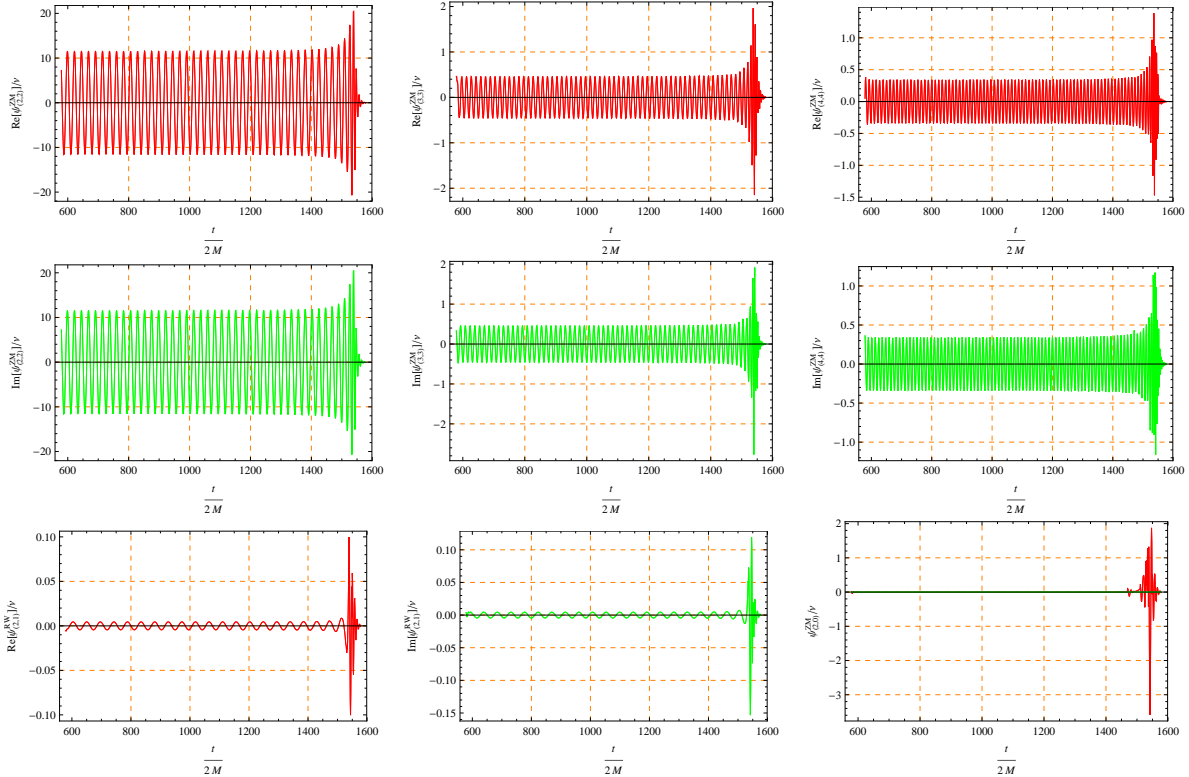


Fig. 4: Top row: Re parts (red) of the amplitudes ψ_{ZM}^l for $l = 2, 3, 4$, magnified by $1/\nu$.
Middle row: Im parts (green) of the same amplitudes.
Bottom row: Re and Im parts of the amplitude ψ_{RW}^{21} , and real amplitude ψ_{ZM}^{20} .

Both the real and imaginary parts are shown, from the time after the spurious transient signals have disappeared. The mode with $m = l = 2$ dominates all others; the modes with $m = l \geq 3$ are subdominant, representing the most important corrections. The modes with $m < l$ are negligible, even for $l = 2$.

Inserting the results for the $\psi_{ZM/RW}^{lm}$ into expression (18) for the gravitational wave amplitude produces the wave forms shown in figs. 5 and 6, as seen from two orthogonal directions in the equatorial plane. The figures show that for about 20 revolutions the signal is almost periodic, ending in a short burst of radiation. The transition from almost-periodic to burst happens in the region where the cross-over from nearly circular to strongly radial motion occurs. Once the mass μ crosses the light ring at $r = 3M$ the gravitational waves apparently red-shift and quickly fade.

The transition in the gravitational wave signal of the ballistic orbit from almost periodic to burst can be identified also in the emitted energy and angular momentum, as is clear from figs. 7. The power peaks at time $t = 1536.5M$, shortly before the compact mass crosses the light ring. The total energy emitted during the infall on a ballistic orbit is a fraction 0.33×10^{-4} of the original energy of motion of the infalling mass. The back reaction from such a small energy loss would only require a very tiny correction to the geodesic motion, as anticipated.

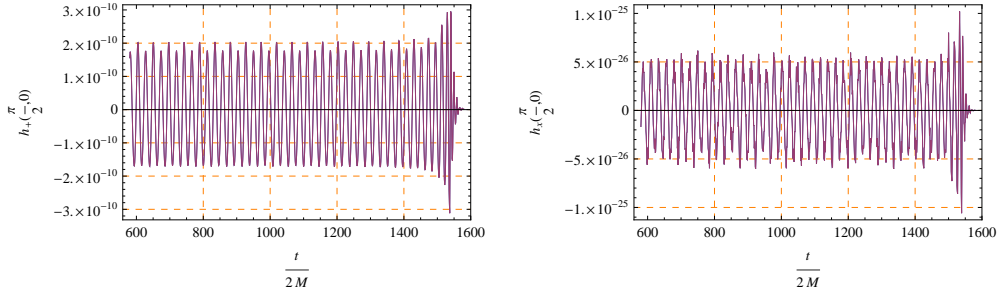


Fig. 5: $h_+(\frac{\pi}{2}, \varphi = 0), h_\times(\frac{\pi}{2}, \varphi = 0)$ polarizations of gravitational waves radiated by a system with mass ratio $\nu = 10^{-7}$ on a ballistic orbit for $e = 0.0015$.

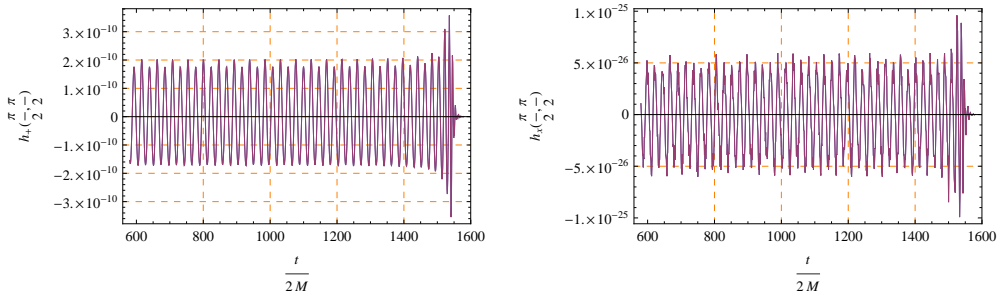


Fig. 6: $h_+(\frac{\pi}{2}, \varphi = \pi/2), h_\times(\frac{\pi}{2}, \varphi = \pi/2)$ polarizations of gravitational waves radiated by a system with mass ratio $\nu = 10^{-7}$ on a ballistic orbit for $e = 0.0015$.

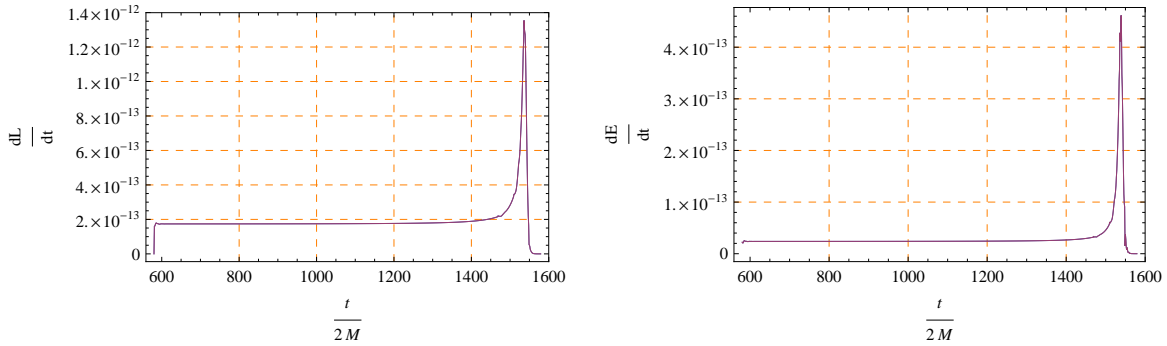


Fig. 7: Angular momentum loss (left) and energy loss (right) on a ballistic orbit with $e = 0.0015$.

5 Discussion

The ballistic orbits (6), (7) are exact solutions of the geodesic equation for Schwarzschild space-time. They describe the motion of a test mass rising up from the horizon to a maximum radial distance $R < 6M$, before returning to the horizon; for R close to $6M$ this includes a large number of turns around the black hole. As they can come arbitrarily close to the ISCO and are degenerate in energy and angular momentum with stable circular orbits, in the limit of small e they can be used to describe test masses infinitesimally

boosted from the ISCO to the infalling part of a ballistic orbit. For such infalling test masses we have computed the gravitational waves emitted during the infall.

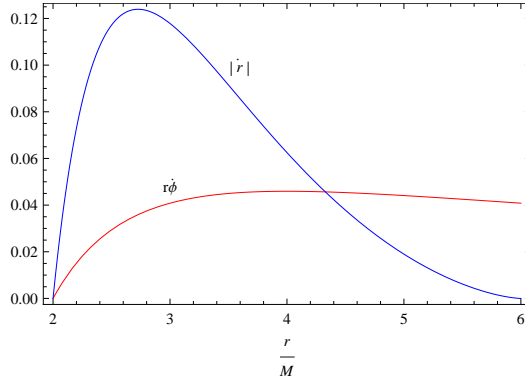


Fig. 8: Evolution of circular and radial velocities as a function of r for the orbit with $\delta = 0.001$; the cross-over occurs at $r_* = 4.328M$.

The merger phase of ballistic EMRs, characterized by an energy and an angular momentum only slightly higher than those on the ISCO, is divided into two phases. First the point mass μ follows an almost-circular orbit, for which $\dot{r} \ll r\dot{\phi}$. Near $r = 4.3M$ the radial and circular velocities become equal, and after this cross-over the radial motion dominates; see fig. 8. This subdivision in the orbit was already recognized in ref. [19], when studying more general cases of black-hole coalescences.

Our calculations show, that the number of almost circular revolutions depends strongly on the radial distance of the apastron, the point of closest approach to the ISCO. It is convenient to parametrize this radial co-ordinate by $R = 6M(1 - \delta)$; equivalently

$$\delta = \frac{2}{3}e. \quad (20)$$

In contrast the radial distance r_*/M where the cross-over occurs, and the number of turns during the second phase of radially dominated motion (the change in orbital phase in units of 2π) are virtually independent of δ . These conclusions are illustrated by the numbers in table 1, calculated from our analytic formulae.

$\delta \times 10^3$	r_*/M	n_1	n_2
1.3	4.328	18.71	0.49
3.2	4.328	11.59	0.50
7.8	4.328	7.09	0.50
18.3	4.327	4.29	0.50
41.2	4.323	2.53	0.50

Table 1: Circular vs. radial phase on ballistic orbits; r_* is the radial co-ordinate at which the cross-over occurs; n_1 is the number of turns in the orbit before reaching the cross-over; n_2 is the number of turns between cross-over and horizon.

The first phase is characterized by almost-periodic gravitational radiation, very similar to the waves emitted by a compact mass in orbit on the ISCO. The second phase instead is much shorter and characterized by a burst of gravitational radiation in which the amplitude increases by a factor of two before the mass disappears effectively behind the light ring.

One can calculate from expressions like (16) the time elapsed during plunge, from the apastron to the horizon $r = 2M$, and this time can vary in a range of values $\frac{t}{2M} \in [60, 1000]$ for $\delta \in [10^{-3}, 10^{-1}]$. Obviously this range of values is determined largely by the duration of the nearly-circular phase of the orbit. It is also evident from the gravitational-wave signal; a comparison of the dominant component of the Regge-Wheeler modes for various values of δ as in fig. 9 shows quite similar final bursts of radiation, whilst the duration of the almost-periodic part of the signal varies considerably [26, 28, 29].

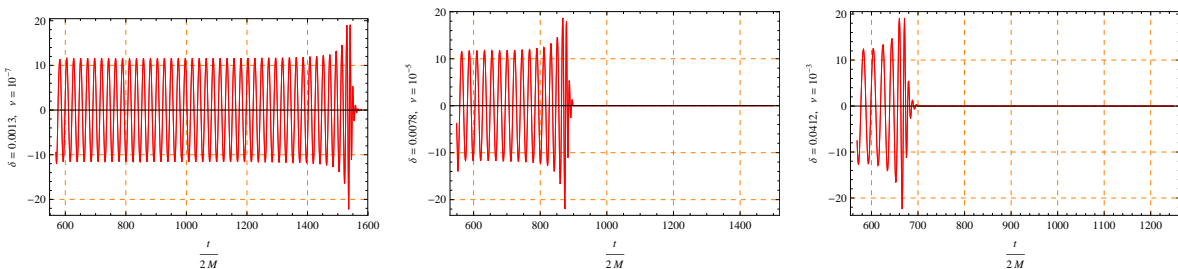


Fig. 9: $\psi_{ZM}^{(2,2)}/\nu$ amplitudes for $\delta = (0.0013, 0.0078, 0.0412)$, only real parts shown. The values of δ are chosen to match mass ratios $\nu = (10^{-7}, 10^{-5}, 10^{-3})$. The smaller (ν, δ) , the longer the near-circular phase after $\frac{t}{2M} = 550$.

In specific parameter ranges the ballistic orbits can be used as a first approximation to the infall phase of an EMR binary. Comparing the wave forms for ballistic orbits with those computed for direct infall from the ISCO³, based on Post-Newtonian and Effective One-Body approximations [26]-[29], it is easy to see that they share the same qualitative behaviour.

For a more precise quantitative comparison we have to tune δ carefully. In fact in [19, 29] it has been shown that the number of revolutions during plunge from the ISCO for coalescences is roughly $\sim (4\nu)^{-1/5}$, where $\nu = \frac{\mu}{M}$ is the mass ratio. The mechanism behind this dependence is the fractional loss of energy by emission of gravitational radiation. As the ballistic orbits are exact geodesics, they do not account for such energy loss, but we can tune δ to make up for this and obtain a realistic approximation. For example, $\nu = 10^{-7}$ corresponds to 19 revolutions and $\delta = 0.0013$. In fig. 9 the mode amplitude for $l = m = 2$ is shown for values of δ matching with $\nu = (10^{-7}, 10^{-5}, 10^{-3})$, respectively.

As a check on these results, we can compare with another result of [19], elaborated in [26], stating that the onset of universal behaviour starts inside the ISCO at co-ordinate distance

$$\frac{r}{M} = 6 - \alpha\nu^{2/5}, \quad (21)$$

³The ISCO is commonly regarded to be the region where the transition from adiabatic inspiral and plunge takes place [19, 27, 29].

where α is a constant. As the ballistic orbits are geodesic and universal, we should expect the values of δ to scale in the same way: $\delta = \gamma\nu^{2/5}$. We find that this relation holds reasonably well with $\gamma = 0.8$ for small values $\nu \leq 10^{-5}$, beyond which deviations arise of the order of 10% or more. Table 2 summarizes the numerical results for this comparison.

$\delta \times 10^3$	ν	$\gamma = \nu^{-2/5}\delta$
1.3	10^{-7}	0.82
3.2	10^{-6}	0.80
7.8	10^{-5}	0.78
18.3	10^{-4}	0.73
41.2	10^{-3}	0.67

Table 2: Test of the universality of the dependence of δ on the mass ratio ν .

Deviations for larger mass ratios are to be expected for at least two reasons: the center-of-mass motion and back reaction of the compact object on the Schwarzschild background geometry have been neglected in our treatment; and the kinetic energy of the compact object is overestimated according to eq. (9) by a factor $\Delta\varepsilon/\varepsilon = 3\delta/8$.

For ballistic orbits in EMR binaries – similar to what is believed to happen for more general cases – the total energy emitted during infall is only a tiny fraction of the initial energy. Therefore in practice we expect the deviation from geodesic motion to be small. Indeed, it has been argued in the literature before [19] that in the particle limit $\nu \rightarrow 0$ the motion is driven mainly by the central black hole, leading to quasi-geodesic motion. Moreover, the energy emission is far too weak to exceed the potential barrier created by the Zerilli potential (18), which shows a maximum in the region close to the light-ring $r \simeq 3M$. Thus the final burst of gravitational waves reaching a distant observer occurs before the compact mass crosses this barrier. No substantial amount of radiation coming from the inner region $r < 3M$ can be transmitted to the outer region [27, 30, 31, 32].

To summarize, we have explored the nature of ballistic orbits in Schwarzschild space-time, and established their degeneracy in the (ε, ℓ) -plane with circular orbits. We have computed gravitational wave signals for compact objects falling towards the horizon on such an orbit. We have also argued that ballistic orbits with apastron close to $6M$ can provide good first approximations to infall from bound orbits, in particular from the ISCO. Finally, we have confirmed earlier calculations that the total amount of energy converted into gravitational waves during the plunge phase is small, and that a quasi-geodesic description of this process for EMR binaries seems adequate.

The results reported here can be improved further by computing perturbative corrections to the orbits by the method of geodesic deviations, as was done for the quasi-periodic motion during the inspiral phase in refs. [13, 14].

Acknowledgements

The authors acknowledge useful correspondence with Maarten van de Meent of the University of Southampton. The research reported in this paper is supported by the programme on Gravitational Physics of the Foundation for Fundamental Research of Matter (FOM).

A Source terms in the wave equation

The expressions for the source terms in the Zerilli-Moncrief and Regge-Wheeler equations for an infalling mass on a ballistic orbit can be evaluated using the decomposition into tensor-spherical harmonics as described in detail in refs. [17] and [15]. In the point-particle limit the source terms are concentrated on the world-line of the particle, producing delta-functions and their derivatives. In Schwarzschild space-time the angular modes then take the form

$$\bar{S}_{ZM/RW}^{lm} = \left(1 - \frac{2M}{r}\right) \left(F_{ZM/RW}^{lm} \partial_r \delta(r - r_p) + G_{ZM/RW}^{lm} \delta(r - r_p)\right). \quad (22)$$

The expressions for the coefficient functions F^{lm} and G^{lm} are provided below for the ZM and RW cases separately. For computational convenience the results are given in terms of the rescaled eccentricity $\delta = 2e/3$, as defined in eq. (20).

Zerilli-Moncrief modes

The even modes of the gravitational wave potentials are calculated from the Zerilli-Moncrief equation; the corresponding source terms are

$$F_{ZM}^{lm}(r, \delta, \varphi) = \frac{-24\pi\mu Y^{*lm}\left(\frac{\pi}{2}, \varphi\right)}{(\lambda + 1)\Lambda} \left[\frac{(2M - r)^2 \sqrt{2 - 3\delta + \delta^2} (48M^2(\delta - 1)^2 + r^2(4 - 8\delta + 3\delta^2))}{r^4(9\delta^3 - 36\delta^2 + 44\delta - 16)} \right], \quad (23)$$

and

$$G_{ZM}^{lm}(r, \delta, \varphi) = g_1 Y^{*lm}\left(\frac{\pi}{2}, \varphi\right) + g_2 Z_\varphi^{*lm}\left(\frac{\pi}{2}, \varphi\right) + g_3 U_\varphi^{*lm}\left(\frac{\pi}{2}, \varphi\right) + g_4 V_{\varphi\varphi}^{*lm}\left(\frac{\pi}{2}, \varphi\right), \quad (24)$$

with $g_i = \frac{N_i}{D_i}$, $i = 1, 2, 3$ defined by

$$\begin{aligned} N_1 &= -8\pi\mu \left(1 - \frac{2M}{r}\right) (3\delta - 4) \sqrt{2 - 3\delta + \delta^2} \left[3M(5M - 3r)r^2(4 - 3\delta)^2(3\delta - 2) \right. \\ &+ (4M - r)r^3(4 - 3\delta)^2(3\delta - 2)\lambda + r^4(4 - 3\delta)^2(3\delta - 2)\lambda^2 \\ &+ \Lambda \left(8640M^4(\delta - 1)^3 - 6912M^3r(\delta - 1)^3 + 2Mr^3(112 - 336\delta + 306\delta^2 - 81\delta^3) \right. \\ &\left. \left. + 108M^2r^2(15\delta^3 - 47\delta^2 + 48\delta - 16) + r^4(54\delta^3 - 189\delta^2 + 204\delta - 68) \right) \right. \\ &\left. - r(r + 6M(\delta - 1))(12M(1 - \delta) + r(3\delta - 2))^2\Lambda^2 \right], \\ D_1 &= 3(2M - r)r^4(4 - 3\delta)^2(\delta - 2)(\delta - 1)(3\delta - 2)(1 + \lambda)\Lambda^2, \end{aligned}$$

$$N_2 = -128\sqrt{3}\pi\mu(r-2M)M\sqrt{(r+6M(\delta-1))(\delta-2)}(\delta-1)(12(1-\delta)M+r(3\delta-2)),$$

$$D_2 = l(l+1)r^3\sqrt{r^3}(3\delta-4)(4-8\delta+3\delta^2)\Lambda,$$

$$N_3 = -1152M^2\pi\mu(r-2M)^2(\delta-1)^3,$$

$$D_3 = r^6(1+\lambda)\Lambda(3\delta-4)(3\delta-2)\sqrt{2-3\delta+\delta^2},$$

$$N_4 = -4608M^2\pi\mu(2M-r)(\delta-1)^3,$$

$$D_4 = r^4(3\delta-4)(3\delta-2)\sqrt{2-3\delta+\delta^2}\frac{(l-2)!}{(l+2)!}.$$

Regge-Wheeler modes

The odd modes of the gravitational wave potentials are calculated from the Regge-Wheeler equation; the corresponding source terms are

$$F_{RW}^{lm}(r, \delta, \varphi) = \frac{2304M^2\pi\mu(\delta-1)^2\sqrt{2-3\delta+\delta^2}(r-2M)^2(l-2)!}{r^5(9\delta^3-36\delta^2+44\delta-16)(l+2)!} W_{\varphi\varphi}^{*lm}\left(\frac{\pi}{2}, \varphi\right), \quad (25)$$

and

$$G_{RW}^{lm}(r, \delta, \varphi) = -M\pi\mu \left[\frac{9216M(r-3M)(r-2M)(\delta-1)^2(l-2)!}{r^6(9\delta^3-36\delta^2+44\delta-16)(l+2)!} W_{\varphi\varphi}^{*lm}\left(\frac{\pi}{2}, \varphi\right) \right. \\ \left. + \frac{64\sqrt{3}(r-2M)(\delta-1)^2(12M(1-\delta)+r(3\delta-2))\sqrt{\frac{r+6M}{r^3(\delta-2)(\delta-1)}}}{l(l+1)r^4(3\delta-4)(3\delta-2)} X_{\varphi}^{*lm}\left(\frac{\pi}{2}, \varphi\right) \right]. \quad (26)$$

References

- [1] K. Somiya [KAGRA Collaboration], *Detector configuration of KAGRA: The Japanese cryogenic gravitational-wave detector*, *Class. Quant. Grav.* **29** (2012) 124007 [arXiv:1111.7185 [gr-qc]]
- [2] T. Accadia *et al.* [Virgo Collaboration], *Calibration and sensitivity of the Virgo detector during its second science run*, *Class. Quant. Grav.* **28** (2011) 025005 [Erratum-ibid. **28** (2011) 079501] [arXiv:1009.5190 [gr-qc]].
- [3] P. A. Seoane *et al.* [eLISA Collaboration], *The Gravitational Universe*, arXiv:1305.5720 [astro-ph.CO].
- [4] T. Damour
The general relativistic two body problem,
arXiv:1312.3505 [gr-qc] (2013).
- [5] B.S. Sathyaprakash, B.F. Schutz
Physics, Astrophysics and Cosmology with Gravitational Waves,
Living Reviews in Relativity **2** (2009).
- [6] S. Chandrasekhar
The Mathematical Theory of Black Holes
Clarendon Press, Oxford (1983)
- [7] C.W. Misner, K.S. Thorne and J.A. Wheeler
Gravitation
Freeman, San Francisco (1970)
- [8] J.B. Hartle
Gravity
Addison Wesley, San Francisco (2003)
- [9] T. Futamase and Y. Itoh
The Post-Newtonian Approximation for Relativistic Compact Binaries,
<http://www.livingreviews.org/lrr-2007-2>
- [10] M. Maggiore
Gravitational Waves. Volume 1: theory and experiments
Oxford University Press (2007)
- [11] A. Balakin, J.W. van Holten and R. Kerner
Motions and world-line deviations in Einstein-Maxwell theory
Class. Quantum Grav. **17** (2000), 5009; arXiv:gr-qc/0009016

- [12] R. Kerner, J.W. van Holten, R. Colistete Jr.
Relativistic Epicycles: another approach to geodesic deviations
Class. Quantum Grav. 18 (2001), 4725; arXiv:gr-qc/0102099
- [13] G. Koekoek and J.W. van Holten
Epicycles and Poincaré Resonances in General Relativity
Phys. Rev. D 83:064041 (2011); arXiv:1011.3973v1 [gr-qc]
- [14] G. Koekoek and J.W. van Holten
Geodesic deviations: modeling extreme mass-ratio systems and their gravitational waves
Class. Quantum Grav. 28 (2011), 225022; arXiv:1103.5612 [gr-qc]
- [15] G. Koekoek
The Geodesic Deviation Method and Extreme Mass-Ratio Systems
PhD thesis, VU University (Amsterdam, 2011)
- [16] K. Martel and E. Poisson
Phys. Rev. D 66:084001 (2002);
Gravitational perturbations of the Schwarzschild spacetime: a practical covariant and gauge-invariant formalism, Phys Rev D 71:104003 (2005)
- [17] K.Martel
Particles and black holes: time-domain integration of the equations of black-hole perturbation theory
Phd thesis, The University of Guelph, Guelph (2004)
- [18] C.Cutler, D.Kennefick and E.Poisson
Phys. Rev. D 50 (1994), 3816.
- [19] A.Buonanno, T.Damour
Transition from inspiral to plunge in binary black hole coalescences
Phys. Rev. D 62:064015 (2000)
- [20] T. Regge and J.A. Wheeler
Stability of a Schwarzschild Singularity
Phys. Rev. 108 (1957), 1063
- [21] F.J. Zerilli
Effective Potential for Even-Parity Regge-Wheeler Gravitational Perturbation Equations
Phys. Rev. Lett. 24 (1970), 737
- [22] V. Moncrief
Gravitational perturbations of spherically symmetric systems I. The exterior problem.
Ann. Phys. 88 (1974), 323

- [23] C.O. Lousto and R.H. Price
Understanding initial data for black hole collisions
Phys. Rev. D 56 (1997), 6439.
- [24] S.Hopper, C.Evans
Gravitational perturbations and metric reconstruction: Method of extended homogeneous solutions applied to eccentric orbits on a Schwarzschild black hole
Phys.Rev. D 82: 084010 (2010)
- [25] A. Nagar, T. Damour, A. Tartaglia
Binary black hole merger in the extreme mass ratio limit
Class. Quantum Grav. 24 S109 (2007)
- [26] S. Bernuzzi, A. Nagar
Binary black hole merger in the Extreme Mass-Ratio limit: a multipolar analysis
Phys. Rev. D 81:084056, arXiv:1003.0597v2 [gr-qc] (2010)
- [27] T.Damour, A.Nagar, S. Bernuzzi
Improved effective-one-body description of coalescing nonspinning black-hole binaries and its numerical-relativity completion
Phys. Rev. D 87:084035 (2013)
- [28] M.A.Scheel, M.Boyle et al.
High-accuracy wave forms for binary black hole inspiral, merger, and ringdown
Phys. Rev. D 79:024003 (2009)
- [29] T.Damour, A.Nagar
Faithful Effective-One-Body wave forms fo small-mass ratio coalescing black-hole binaries
Phys. Rev. D 76:064028 (2007)
- [30] E. Berti et al.
Inspiral, merger and ringdown of unequal mass black hole binaries: A multipole analysis
Phys. Rev. D 76:064034 (2007)
- [31] M.Davis, R.Ruffini, W.H.Press, H.R.Price
Gravitational Radiation from a particle falling radially into a Schwarzschild Black Hole
Phys. Rev. Lett. 27, 1466 (1971)
- [32] S. Bernuzzi, A. Nagar, A Zenginoglu
Binary black hole coalescence in the extreme-mass-ratio limit
Phys. Rev. D 83:064010 (2011)